Handling Target Obscuration through Markov Chain Observations

Michael A. Kouritzin and Biao Wu

Department of Mathematical and Statistical Sciences
University of Alberta
Edmonton, Alberta, Canada

ABSTRACT

Target Obscuration, including foliage or building obscuration of ground targets and landscape or horizon obscuration of airborne targets, plagues many real world filtering problems. In particular, ground moving target identification Doppler radar, mounted on a surveillance aircraft or unattended airborne vehicle, is used to detect motion consistent with targets of interest. However, these targets try to obscure themselves (at least partially) by, for example, traveling along the edge of a forest or around buildings. This has the effect of creating random blockages in the Doppler radar image that move dynamically and somewhat randomly through this image.

Herein, we address tracking problems with target obscuration by building memory into the observations, eschewing the usual corrupted, distorted partial measurement assumptions of filtering in favor of dynamic Markov chain assumptions. In particular, we assume the observations are a Markov chain whose transition probabilities depend upon the signal. The state of the observation Markov chain attempts to depict the current obscuration and the Markov chain dynamics are used to handle the evolution of the partially obscured radar image. Modifications of the classical filtering equations that allow observation memory (in the form of a Markov chain) are given. We use particle filters to estimate the position of the moving targets. Moreover, positive proof-of-concept simulations are included.

Keywords: Target Identification, Target Obscuration, Tracking Problem, Random Blockage, Classical Filter Equation, Particle Filter

1. INTRODUCTION

We assume that there is a random number N_t of ground moving targets, where $N_t \in \{0, 1, 2, 3\}$, to be detected and tracked. The area over which the targets (e.g., military tanks) move, is observed by Doppler radar mounted on a spy plane or unmanned aerial vehicle. However, the detection and tracking problem are complicated by the facts that the radar reading are subject to random interference and the targets try to obscure themselves by moving along the edge of forests or around buildings. The landscape or horizon may obscure the observations of the targets too. These obscurations create random blockages in the Doppler radar image. Spatial noise and sensor truncation effects corrupt or distort the measurement of the radar image as well. The confined randomness described herein is so large that we can not estimate the position of the moving target by a small number of images. However, with enough knowledge of the characteristics of the ground moving targets, we can keep the track of the state of the target based upon a sequence of radar images over a time interval. We do not preprocess the images before we provide the observations to the particle filter algorithm.

Further author information: (Send correspondence to B.W.)
M.A.K: E-mail: mkouritz@math.ualberta.ca, Telephone: 1 780 492 0215
B.W: E-mail: bwu@math.ualberta.ca, Telephone: 1 780 492 4394

Signal Processing, Sensor Fusion, and Target Recognition XVII, edited by Ivan Kadar
Proc. of SPIE Vol. 6968, 69680S, (2008) · 0277-786X/08/$18 · doi: 10.1117/12.779837

1.1 Blockages Description

To make the models considered here simple and simulations not too complicated, we consider the ground to be flat.

In a typical battlefield, ground moving targets always try to avoid the surveillance from Doppler-radar-equipped drones by moving along the edge of forests or around buildings. Different forests consist of various trees, bushes or shrubs. In particular, each forest may have its own density of trees, bushes or shrubs which might be very different from that of others. Therefore, when we consider forests as one source of blockages for the ground moving targets, we should classify forests into different types. For each forest, the capability of blocking electromagnetic signals varies with seasons as the density of foliage varies.The second source of blockage for ground moving targets, buildings, have assorted shapes. We may also classify the buildings into different types based on their shape characteristics. Dissimilar to forests, we assume that buildings may completely block electromagnetic signals in all seasons.

In our proof-of-concept simulations, we give four types of forests by their shapes: **Rectangle**, **L** shape, **T** shape, and **Random** shape. The last shape of forests is determined by a polygon with random number of vertices and random locations. We simulate five types of buildings by their shapes: **Rectangle**, **L** shape, **T** shape, and **X** shape, and **U** shape. The common geometric feature of those blockages including forest blockages and building blockages is that they are polygons which are convex or concave. A very simple and extremely efficient algorithm has been developed to draw an arbitrary polygon.

A drone is usually small, with no passengers in it. Consequently, a drone is designed to have more flexibility in flying than a manned aerial vehicle does, and the drone does not fly as steadily as a manned airplane. Hence, the jitters of the drone and other atmospherical factors, like turbulence, make it difficult for the Doppler radar to recognize immediately the type of certain blockage when it begins to enter the horizon of the Doppler radar. In other words, the radar image of the boundary of a blockage may look like being random, and we can not tell the type of a blockage until we have consecutive images of the blockage when the drone is approaching the blockage.

One may wonder why we did not model the blockages as part of the signal. The main reasons are computational. Including them into the signal necessarily increases its dimensionality significantly so much so that the problem could not be solved using particle filters. Fortunately, we do not have to include them in the signal but rather can put them in the observations. One of the main purposes of this paper is to show how to include them in the observations.

1.2 Targets Description

The ground moving targets here are assumed to be military tanks. We assume that for a tank, the ratio of length and width is approximately 2:1 with length 8 meters and width 4 meters. Characteristics of tanks are ignored except its length, width, maximum county speed, acceleration.

We assume that the j^{th} target has six state parameters: x_t^j, y_t^j, θ_t^j, $\dot{\theta}_t^j$, $\dot{f}_t^j$ and χ_t^j $(1 \le j \le 3)$. Here parameters x_t^j and y_t^j indicate its x- and y- coordinates, and θ_t^j denotes its orientation at time t. Parameter $\dot{\theta}_t^j$ represents the rate of change of θ_t^j and $\dot{f}_t^j$ scalar velocity in the forward direction at time t. We have the following relation,

$$\begin{bmatrix} \dot{x}_t^j \\ \dot{y}_t^j \end{bmatrix} = \begin{bmatrix} \dot{f}_t^j \cos\theta_t^j \\ \dot{f}_t^j \sin\theta_t^j \end{bmatrix}, \tag{1}$$

where $\dot{x}_t^j$ and $\dot{y}_t^j$ indicate the rate of change of x_t^j and y_t^j. The sixth parameter χ_t^j denotes the current maneuver type from the possible set of {moving forward, turning left, turning right, stopping}. Stopping is viewed as a maneuver type because a moving target might stop as planned due to military tasks or unexpectedly due to technical reasons like overheat. We allow the position of (x_t^j, y_t^j) to be in the set $S = [0, 400] \times [0, 1600]$, here one unit means one meter. If a target leaves this domain through its stochastic evolution, it will be removed from consideration, and the number of targets N_t will be decremented by one. For $j = 1, 2, \cdots, N_t$, we let

$$X_t^j = (x_t^j, y_t^j, \theta_t^j, \dot{\theta}_t^j, \dot{f}_t^j, \chi_t^j) \tag{2}$$

denote the state of one of the target under consideration in its state space $S_0 = S \times \mathbb{R}^2 \times [0, 80] \times \{1, 2, 3, 4\}$. To keep track of all targets under consideration without knowledge of which target is which, we let

$$\mathbb{X}_t(\cdot) = \sum_{j=1}^{N_t} \delta_{X_t^j}(\cdot) \tag{3}$$

denote the signal measure on S_0. This contains complete information about the state of the collection of targets $(X_t^1, \cdots, X_t^{N_t})$.

2. SIGNAL MODEL

2.1 Attraction-Repulsion Field

We introduce the following attraction-repulsion field to reflect the weak interaction among the moving targets. The notion of attraction-repulsion has been used in.[4] Our definition here shares some similarities with that in.[4] Assume that s_1 and s_2 are two moving targets. Based on our previous description, both s_1 and s_2 are rectangles. To define the attraction-repulsion between s_1 and s_2 precisely, we do not simply refer to s_1 and s_2 as two points, or consider only the centers of s_1 and s_2 but rather consider the "two closest points" of s_1 and s_2, one point from s_1 and another from s_2.

The "two closest points" are determined by simple geometric knowledge. Since s_1 and s_2 are both rectangles which do not intersect with each other, that is to say, collision of one moving target with another is prohibited, there always exists the positive shortest distance between s_1 and s_2. It can be proved that the shortest distance can always be attained by choosing one vertex from s_1 or s_2 to another point from the boundary of s_2 or s_1. The "two closest points" are so picked. Those two points might not be unique, we are interested in only the pairs determined by computer algorithms.

Next, we define the attraction-repulsion between the "two closest points" of s_1 and s_2. We also use s_1 and s_2 to represent their "two closest points" when they cause no confusion. Let

$$\Pi(s_1, s_2) = \sqrt{|\pi_x(s_1) - \pi_x(s_2)|^2 + |\pi_y(s_1) - \pi_y(s_2)|^2}, \tag{4}$$

where π_x and π_y denote projection onto the x and y components. Then, we let

$$\kappa(s_1, s_2) = \begin{cases} 0 & s_1 = s_2 \\ \frac{10000}{(\Pi(s_1,s_2)+\epsilon)^2} - \frac{30000}{4(\Pi(s_1,s_2)-\epsilon)} & s_1 \neq s_2 \end{cases}, \tag{5}$$

$$\kappa_x(s_1, s_2) = \kappa(s_1, s_2) \frac{\pi_x(s_1) - \pi_x(s_2)}{\Pi(s_1, s_2)}, \tag{6}$$

$$\kappa_y(s_1, s_2) = \kappa(s_1, s_2) \frac{\pi_y(s_1) - \pi_y(s_2)}{\Pi(s_1, s_2)}. \tag{7}$$

This field has the effect of drawing a target slightly toward another if it is distant and repelling it from any other to which it becomes too close. We choose $\epsilon = 8$ to be the closest distance that one target should come to another.

This attraction-repulsion is enacted by the following variables:

$$\phi_t^{r,j} = \sqrt{\int |\kappa(z, X_t^j)|^2 \mathbb{X}_t(dz)}, \tag{8}$$

and

$$\phi_t^{\theta,j} = \arctan(\int \kappa_y(z, X_t^j) \mathbb{X}_t(dz), \int \kappa_x(z, X_t^j) \mathbb{X}_t(dz)), \tag{9}$$

which denotes the strength and orientation of the deflecting force. Here, $\arctan(\cdot, \cdot)$ is a two-parameters arctangent function with range $[0, 2\pi)$, and is different from the usual one-parameter arctangent function $\arctan(\cdot)$ with range $(-\frac{\pi}{2}, \frac{\pi}{2})$. $\arctan(x, y)$ can determine the arc angle between the line segment from the origin to point (x, y) and x-axis wherever (x, y) locates in the four quadrants and $\arctan(y/x)$ can not.

2.2 Maneuver Type

The state space of the Markov chain χ_t^j is $\{1,2,3,4\}$, denoting the four maneuver types *moving forward, turning left, turning right, stopping* respectively. The rates of changing maneuvers are given as follows:

$$\lambda_{j,t}^{1\to 2}(X_t^j,\mathbb{X}_t)=\lambda_{j,t}^{1\to 3}(X_t^j,\mathbb{X}_t)=\lambda_{j,t}^{1\to 4}(X_t^j,\mathbb{X}_t)=\frac{1}{8}+100\phi_t^{r,j}, \tag{10}$$

$$\lambda_{j,t}^{2\to 1}(X_t^j,\mathbb{X}_t)=\lambda_{j,t}^{3\to 1}(X_t^j,\mathbb{X}_t)=\lambda_{j,t}^{4\to 1}(X_t^j,\mathbb{X}_t)=\frac{1}{8}+\frac{1}{200\phi_t^{r,j}}, \tag{11}$$

$$\lambda_{j,t}^{2\to 3}(X_t^j,\mathbb{X}_t)=\lambda_{j,t}^{2\to 4}(X_t^j,\mathbb{X}_t)=\frac{1}{5}, \tag{12}$$

$$\lambda_{j,t}^{3\to 2}(X_t^j,\mathbb{X}_t)=\lambda_{j,t}^{3\to 4}(X_t^j,\mathbb{X}_t)=\frac{1}{6}, \tag{13}$$

$$\lambda_{j,t}^{4\to 2}(X_t^j,\mathbb{X}_t)=\lambda_{j,t}^{4\to 3}(X_t^j,\mathbb{X}_t)=\frac{1}{7}. \tag{14}$$

When a moving target is moving towards and becomes too close to another target, the repulsion is so strong that the target has to change its maneuver type from moving forward to avoid collision.

Assume that $\{B^{j,a},B^{j,b},B^{j,c},B^{j,d}\}_{j=1}^{N_t}$ is a collection of independent standard 2-dimensional Brownian motions. The stochastic behavior of the moving targets are described by nonlinear systems which depend on the maneuver type process $\{\chi_t^j, 1\le j\le N_t, t\ge 0\}$. For each value of χ_t^j, the jth moving target is simulated according to the following formulae:

1. **Moving forward** ($\chi_t^j=1$) In this case, the stochastic behavior of the moving target in a field is described by nonlinear system of SDEs as follows:

$$d\begin{bmatrix} \dot{f}_t^j \\ \dot{\theta}_t^j \end{bmatrix}=\begin{bmatrix} \alpha_1(40-\dot{f}_t^j)^\beta \\ \alpha_2(\phi_t^{\theta,j}-\dot{\theta}_t^j)\phi_t^{r,j} \end{bmatrix}dt+\begin{bmatrix} \sqrt{(80-\dot{f}_t^j)\dot{f}_t^j} & 0 \\ 0 & \frac{1}{10}\sqrt{(80-\dot{f}_t^j)\dot{f}_t^j} \end{bmatrix}dB_t^{j,a}, \tag{15}$$

where $\alpha_1>0$, $\alpha_2>0$, $\beta>1$. In this maneuver type, scalar velocity of a moving target has the mean reversion property. The long-time average mean scalar velocity is 40 kilometers per hour and the maximum scalar velocity is 80 kilometers per hour. The attraction-repulsion force significantly affects the angular velocity of a moving target when another is approaching it.

2. **Turning left** ($\chi_t^j=2$) In this case,

$$d\begin{bmatrix} \dot{f}_t^j \\ \dot{\theta}_t^j \end{bmatrix}=\begin{bmatrix} 30-\dot{f}_t^j \\ \gamma-\dot{\theta}_t^j \end{bmatrix}dt+\begin{bmatrix} \sqrt{(60-\dot{f}_t^j)\dot{f}_t^j} & 0 \\ 0 & \frac{1}{10}\sqrt{(60-\dot{f}_t^j)\dot{f}_t^j} \end{bmatrix}dB_t^{j,b}, \tag{16}$$

where $\gamma>0$. Both the forward and angular velocity have the mean reversion property. The mean forward velocity is 30 kilometers per hour and maximum forward velocity 60 kilometers per hour. The mean angular velocity is γ per hour.

3. **Turning right** ($\chi_t^j=3$) In this case,

$$d\begin{bmatrix} \dot{f}_t^j \\ \dot{\theta}_t^j \end{bmatrix}=\begin{bmatrix} 30-\dot{f}_t^j \\ -\gamma-\dot{\theta}_t^j \end{bmatrix}dt+\begin{bmatrix} \sqrt{(60-\dot{f}_t^j)\dot{f}_t^j} & 0 \\ 0 & \frac{1}{10}\sqrt{(60-\dot{f}_t^j)\dot{f}_t^j} \end{bmatrix}dB_t^{j,c}. \tag{17}$$

Here the mean angular velocity is $-\gamma$ per hour.

4. **Stopping** ($\chi_t^j=4$) In this case,

$$d\begin{bmatrix} \dot{f}_t^j \\ \dot{\theta}_t^j \end{bmatrix}=\begin{bmatrix} -\alpha_3\dot{f}_t^j-\alpha_4 \\ -\beta_3\dot{\theta}_t^j-\beta_4 \end{bmatrix}dt+\begin{bmatrix} \sigma_1\dot{f}_t^j & 0 \\ 0 & \sigma_2\dot{\theta}_t^j \end{bmatrix}dB_t^{j,d}, \tag{18}$$

where α_3, α_4, β_3, β_4, σ_1, and σ_2 are nonnegative constants. In this maneuver type, a moving object almost 'linearly' reduces its forward and angular velocities.

3. OBSERVATION MODEL AND ITS SERP FILTER

3.1 Drone and Doppler Radar

The observations of the ground moving targets are made from a Doppler radar mounted on a drone. For simplicity of simulation, we assume that the drone flies with constant altitude over the ground when it is making observations about a specific area with blockages and moving objects described before. We assume that the drone flies with the following formulae:

$$\begin{bmatrix} x_t \\ y_t \end{bmatrix} = \begin{bmatrix} R\cos(\alpha_5 t) + u_t \\ R\sin(\alpha_5 t) + v_t \end{bmatrix}, \tag{19}$$

where $R > 0$, $\alpha_5 > 0$, u and v are Ornstein-Uhlenbeck processes so u_t and v_t are normal random variables with mean 0 and standard deviations $\sigma_3 > 0$ and $\sigma_4 > 0$ respectively. By these equations, the drone flies a circle with radius R and approximate speed $R \cdot \alpha_5$ kilometers per hour.

The Doppler radar makes observations of the ground by producing radar images on a radar screen. In our simulation, we neglect the mechanism of how the Doppler radar works and how the Doppler effect is used to detect moving targets and so on. We focus on only the images generated on the radar screen, ignoring all other scientific and technical details of the process of sending and receiving electromagnetic waves, transferring the electromagnetic signals into radar images. In our observation model formulated below, we do take into account the disturbances from the function of sensors and the whole procedures of producing the images.

3.2 Observation Model

We assume that the observations are made at a sequence of times $\{t_k, k \geq 0\}$ with $t_0 = 0$ and $t_{k+1} - t_k = 0.1$ $(k \geq 0)$ time unit, say, second. Although the Doppler radar has very broad range of detection, we assume in this proof-of-concept work that the radar concentrates only on an area of 200×200 square meters to send and receive clearer electromagnetic waves and process them more efficient and faster. Since the drone flies with the equations (19), the radar image of the observed area moves accordingly on the radar screen. We assume that a pixel on radar screen represents a ground area of 0.8×0.8 square meters, so each radar image is a two-dimensional raster of 250×250 pixels denoted by D_k at time t_k. Let value $Y_k^{(i,j)}$ represent the observation of the (i, j) pixel in the two-dimensional radar raster at time t_k. We define $\{\mathbb{Y}_k = (Y_k^{(i,j)})_{(i,j)\in D_k}\}$ as follows:

$$Y_k^{(i,j)} = h_k^{(i,j)}(\mathbb{X}_{t_k}) + V_k^{(i,j)}, \tag{20}$$

where $h_k^{(i,j)}(\mathbb{X}) = c^{(i,j)} 1_{(i,j)\in A_{\mathbb{X}}}$ and $V_k^{(i,j)}$ is a normal random variable with mean 0 and variance $\sigma_k^{(i,j)}$. The set $A_{\mathbb{X}}$ consists of all points representing the moving objects. We only need to define $c^{(i,j)}$ when (i, j) actually represents a part on moving object surface. If this part hides underneath a blockage building, $c^{(i,j)} = 0$, i.e. the building blocks the part from being detected by Doppler radar. If the part hides among a blockage forest, $c^{(i,j)} = 0.5$, i.e. the forest blocks partial electromagnetic waves. If the part is not covered by any blockage, $c^{(i,j)} = 1$. We define the variances of normal random variables as follows. If a pixel (i, j) represents an area of blockage building, $\sigma_k^{(i,j)} = \sigma_b$; an area of blockage forest, $\sigma_k^{(i,j)} = \sigma_f$; an area of moving object, $\sigma_k^{(i,j)} = \sigma_m$. Finally, if a pixel (i, j) represents an area of ground which is not occupied by blockages or moving objects, $\sigma_k^{(i,j)} = \sigma_g$. Therefore, in $V_k^{(i,j)}$, we included the noises from sensors and observation procedures as well as the obscuration from the ground's allocation.

In (20), we actually defined the observations $\{\mathbb{Y}_k\}$ assuming we knew where the blockages were. This would require us to treat the blockages as part of the signal, making the resulting filtering problem too large for computations. Instead, we follow the basic idea of[6] and treat the observations as a Markov chain. The following result is the key to evaluating the state-dependent transition probability for the chain.

PROPOSITION 3.1. *$\{\mathbb{Y}_k\}$ is a Markov chain with transition probability*

$$P(\mathbb{Y}_{k+1} \in A | \mathbb{Y}_k = y, \mathbb{X}_{t_k} = x) = E[E[E[I_A(\mathbb{Y}_{k+1})|\mathbb{X}_{t_{k+1}}, \mathbb{B}]|\mathbb{X}_{t_k} = x, \mathbb{B}]|\mathbb{Y}_k = y, \mathbb{X}_{t_k} = x], \tag{21}$$

where $\mathbb{B}$ denotes the random configuration of blockages on the ground, x is a realization of all moving objects, y is a realization of radar raster, and A is any Borel set of radar raster.

Proof. First, we have

$$\begin{aligned} P(\mathbb{Y}_{k+1} \in A|\mathbb{Y}_k = y, \mathbb{X}_{t_k} = x) &= E[I_A(\mathbb{Y}_{k+1})|\mathbb{Y}_k = y, \mathbb{X}_{t_k} = x] \\ &= E[E[I_A(\mathbb{Y}_{k+1})|\mathbb{Y}_k = y, \mathbb{X}_{t_k} = x, \mathbb{B}]|\mathbb{Y}_k = y, \mathbb{X}_{t_k} = x]. \end{aligned} \tag{22}$$

Secondly, by (20) and the independence between $\{V_{k+1}^{(i,j)}\}_{(i,j)\in D_{k+1}}$ and $\{V_k^{(i,j)}\}_{(i,j)\in D_k}$ we have

$$\begin{aligned} E[I_A(\mathbb{Y}_{k+1})|\mathbb{Y}_k, \mathbb{X}_{t_k}, \mathbb{B}] &= E[I_A(\mathbb{Y}_{k+1})|\mathbb{X}_{t_k}, \mathbb{B}] \\ &= E[E[I_A(\mathbb{Y}_{k+1})|\mathbb{X}_{t_{k+1}}, \mathbb{X}_{t_k}, \mathbb{B}]|\mathbb{X}_{t_k}, \mathbb{B}] \\ &= E[E[I_A(\mathbb{Y}_{k+1})|\mathbb{X}_{t_{k+1}}, \mathbb{B}]|\mathbb{X}_{t_k}, \mathbb{B}], \end{aligned} \tag{23}$$

where in the last equality, we used the Markov property of $\{\mathbb{X}_{t_k}\}$. (21) follows by (22) and (23). □

In Proposition 3.1, we proved that $\{\mathbb{Y}_k\}$ is a Markov chain related to the filtration $\{\mathscr{F}_k^{\mathbb{XY}} \equiv \sigma(\mathbb{X}_{t_0}, \cdots, \mathbb{X}_{t_k}; \mathbb{Y}_0, \cdots, \mathbb{Y}_k)\}$, given by the signal-observation pairs up to k. In formula (21), we have used the random displacement of blockages to justify the Markov property of $\{\mathbb{Y}_k\}$ related to $\{\mathscr{F}_k^{\mathbb{XY}}\}$. It also provides to us a way of using the particle method to solve the detecting and tracking filter problem. In the sequel, we will also be interested in the information, $\{\mathscr{F}_k^{\mathbb{Y}} \equiv \sigma(\mathbb{Y}_0, \cdots, \mathbb{Y}_k)\}$, generated by the observations up to time k.

3.3 SERP Filter

SERP filter has been used in multi-target tracking problems.[4] The SERP filter for this model is constructed as follows. Based on developments analogous to classical nonlinear filtering theory, to appear elsewhere, we only need to approximate

$$\mu_k(dx) \equiv \frac{\bar{E}[1_{\mathbb{X}_k \in dx}\eta_k|\mathscr{F}_k^{\mathbb{Y}}]}{\bar{E}[\eta_k|\mathscr{F}_k^{\mathbb{Y}}]}. \tag{24}$$

Here $\bar{E}$ denotes the expectation with respect to a reference probability measure $\bar{P}$ and

$$\eta_k = \prod_{j=0}^{k-1} P(\mathbb{Y}_{j+1}|\mathbb{Y}_j, \mathbb{X}_j) \tag{25}$$

is the weighting function. Here $\{\mathbb{X}_k\}$ is independent of $\{\mathbb{Y}_k\}$. Next, we introduce independent signal particles $\{\mathbb{X}_k^i, k = 1, 2, ...\}_{i=1}^{\infty}$. Assuming that each particle has the same law as the signal, we define the weights

$$\eta_k^i = \prod_{j=0}^{k-1} P(\mathbb{Y}_{j+1}|\mathbb{Y}_j, \mathbb{X}_j^i). \tag{26}$$

Then, by deFinnetti's theorem and the law of large numbers we have that

$$\frac{1}{N}\sum_{i=1}^{N} \eta_k^i \delta_{\mathbb{X}_k^i}(dx) \Rightarrow \mu_k(dx). \tag{27}$$

Finally, we convert back to the original measure

$$P(\mathbb{X}_k \in dx|\,\mathscr{F}_k^{\mathbb{Y}}) = \frac{\mu_k(dx)}{\mu_k(1)}. \tag{28}$$

Therefore, we have

$$E(\mathbb{X}_k|\mathscr{F}_k^{\mathbb{Y}}) = \frac{\int x\mu_k(dx)}{\mu_k(1)} \approx \frac{\frac{1}{N}\sum_{i=1}^{N} \eta_k^i \mathbb{X}_k^i}{\frac{1}{N}\sum_{i=1}^{N} \eta_k^i}. \tag{29}$$

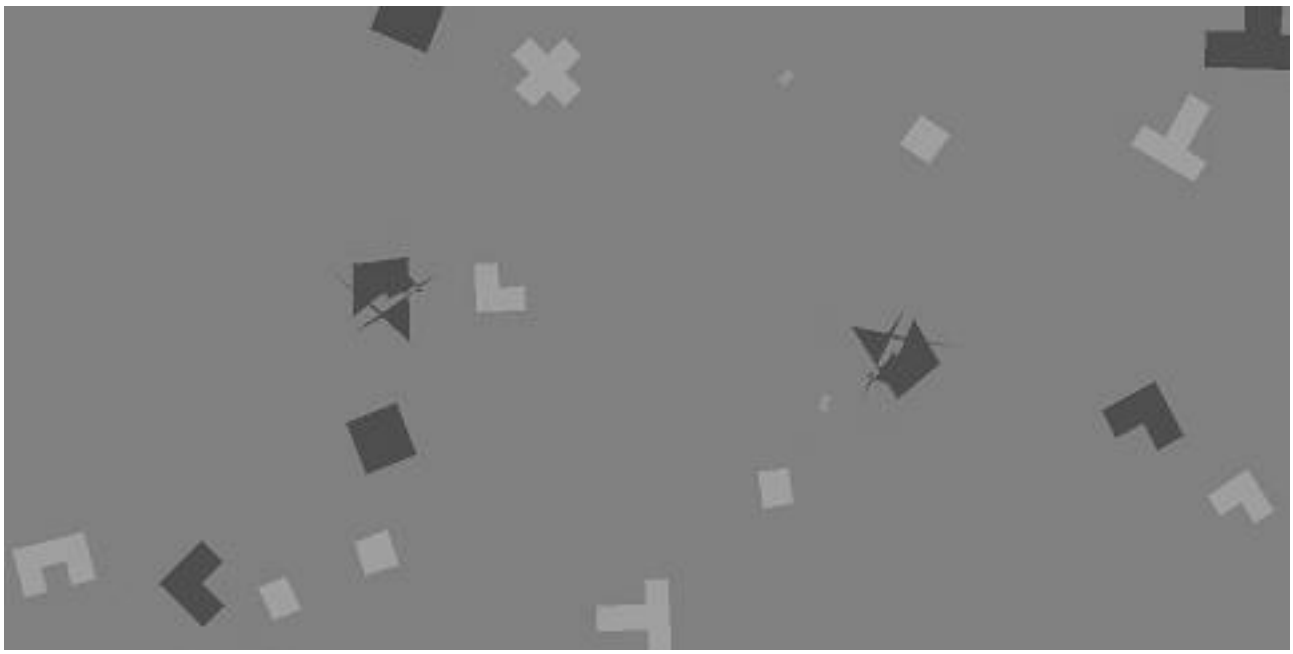

Figure 1. This picture illustrates one half of a typical ground configuration. In this picture, blockages with green color are forests. The forest which looks weird is a random forest mentioned before; it is completely determined by its vertices. The blockages with grey color are buildings. There are two moving objects which are small rectangles.

4. SIMULATION

4.1 Ground Initialization

As mentioned subsection 1.1, we have 4 types of forest blockages and 5 types of building blockages. Each blockage is determined by all its vertices and has random number of copies. Each blockage is randomly configured on the ground by randomly choosing its center and its orientation. An algorithm is established to exclude overlapping of blockages. The moving targets are also randomly displayed on the ground, with their states being random as well. One half of a typical ground configuration is illustrated by Figure 1.

4.2 Approximate State-Dependent Transition Probability

By Proposition 3.1, we have built observation memory into the Markov chain $\{\mathbb{Y}_k\}$ through $\mathbb{B}$. We approximate the distribution of the random blockages $\mathbb{B}$ by randomly selecting $\mathbb{B}$ from a finite number N of configurations $\{B_i\}_{i=1}^N$, which contain the true displacement of blockages around which the ground targets move. Note that once a configuration of blockages is selected, a ground map is also determined. One way of looking at our problem is through random maps: The original problem has an uncoubtable number of random maps consisting of all possible blockage configurations and we replace that with a finite number of statistically-appropriately-chosen maps. We do not try to determine which map we have but rather include their traces in the observation Markov chain. The cost of this approach is that all blockage information is lost after it leaves the observation area. However, more importantly, the problem becomes computationally feasible.

There is another advantage to our random map approach: A spy plane can be equipped with ground maps taken from satellites. However, due to jitter etc. one is never sure which map to use nor exactly how to orient it. In this case, one can just make $\mathbb{B}$ a random selection of these maps and orientation for it.

To implement SERP filter on this target obscuration problem, we need an efficient way to compute the state-dependent transition probability , which is given by formula (30). To avoid tremendous computation problem, we assume that $\mathbb{B}$ has only $N = 20$ configurations for this proof-of-concept work, but we do not

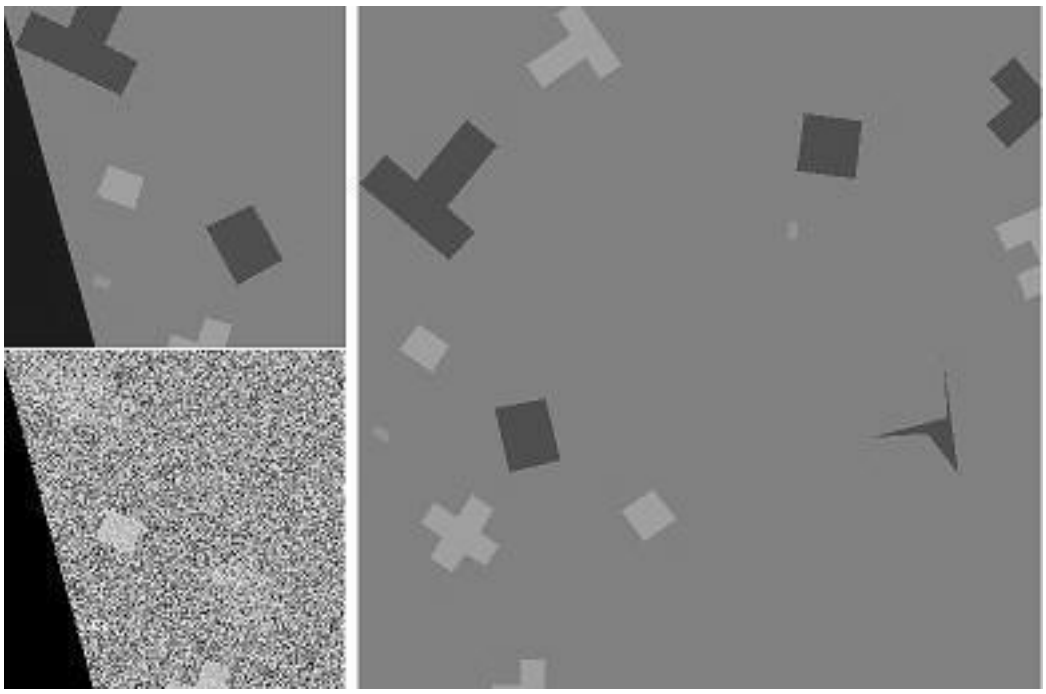

Figure 2. One quarter of a ground configuration is given on the right hand side of this picture. The left above corner is the part of the ground observed by the Doppler radar and the left below part is the observation radar raster. In this picture, the drone is largely flying from west to east and entering into the ground. The blue or black wedge represents an area which is not a part of the ground and neglected by our simulation.

assume a particular distribution of $\mathbb{B}$. So we need to do sampling to obtain the empirical distribution of $\mathbb{B}$. Although we have closed forms given by (15), (16), (17) and (18) of $\{\mathbb{X}_{t_k}\}$, it is not a easy matter to compute $E[E[I_A(\mathbb{Y}_{k+1})|\mathbb{X}_{t_{k+1}}, B_i]|\mathbb{X}_{t_k} = x, B_i]$ for given B_i directly. Instead, we also sample on the conditional distribution of $\mathbb{Y}_{k+1}$, given $\mathbb{X}_{t_k} = x$ and B_i. Thus, we have the following executable equation:

$$\begin{aligned} & P(\mathbb{Y}_{k+1} \in A|\mathbb{Y}_k = y, \mathbb{X}_{t_k} = x) \qquad (30) \\ = \quad & \frac{1}{NM}\sum_{i=1}^{N}\sum_{j=1}^{M} P(\mathbb{Y}_{k+1} \in A|\mathbb{X}_{t_{k+1}} = z_j, B_i)P(\mathbb{X}_{t_{k+1}} = z_j|\mathbb{X}_{t_k} = x, B_i), \end{aligned}$$

where M is the sample size to compute the empirical distribution of $\mathbb{Y}_{k+1}$, given $\mathbb{X}_{t_k} = x$ and B_i.

Herein, we use the established method to compute the mean squared error (MSE) of this filtering problem, see.[4] We also use the simplification method suggested in.[2] Specifically, for each observation, we only do the major calculation on the whole raster once and for each particle, we only refer to those raster pixels that are within the targets of that particle. In particular, since the radar observes only a small part of the referred ground and it takes time for the drone to pass through the ground, we only compute the weights for those particles which enter into the observation of the radar, and let those particles which are out of the observation of radar screen evolving only. In Figure 2, we illustrate one quarter of a ground configuration, the area observed by a Doppler radar and its corresponding observation image. In the following table, we give the mean squared error with respect to the number of targets in simulations and the simulation time. Mean squared error were computed at the observation time sequence $\{t_k, k \geq 0\}$ with $t_0 = 0$ and $t_{k+1} - t_k = 0.1$ second, but we only give the numbers at every two seconds.

Simulation Time (seconds)	2	4	6	8	10	12	14	16
1-Target Mean Squared Error	8.5	6.7	8.4	50.9	10.3	6.2	5.1	4.6
2-Target Mean Squared Error	19.3	16.7	75.9	43.6	22.7	87.2	13.6	7.8

5. CONCLUSION

The SERP filter shows its power again on detecting and tracking moving targets. The exception cases, as one would imagine, are as follows. 1) During the process of the drone passes through the specific ground, the moving targets fail to enter the observation of Doppler radar. 2) The targets move underneath the building blockages which can completely block the electromagnetic waves away from them, or among the forests which greatly distort the observation of radar. In the latter case, the SERP filter can sometimes detect targets too, but not always. The radar's ability accounts for more exception cases than the SERP filter.

REFERENCES

[1] D. Ballantyne, H. Chan, and M.A. Kouritzin, "A novel branching particle method for tracking", in *Proceedings of SPIE, Signal and Data Processing of Small Targets 2000*, **4048**, pp. 277-287, 2000.

[2] D. Ballantyne, H. Chan, and M.A. Kouritzin, "A branching particle-based nonlinear filter for multitarget tracking", in *Proceedings of the 4th ISIF/IEEE International Conference on Information Fusion (Fusion 2001)*, Montreal, QC, August 2001.

[3] D. Ballantyne, S. Kim, and M.A. Kouritzin, "A weighted interacting particle-based nonlinear filter", in *Signal Processing, Sensor Fusion and Target Recongition XI*, I. Kadar, ed., *Proceedings of SPIE*, **4729**, pp. 236-247, 2002.

[4] D. Ballantyne, J. Hailes, M.A. Kouritain, H. Long, and J. Wiersma, "A hybrid weighted interacting particle filter for multi-target tracking", in *Signal Processing, Sensor Fusion, and Target Recognition XII*, I. Kadar, ed., *Proceedings of SPIE*, **5096**, pp. 244-255, 2003.

[5] T.G. Kurtz and J. Xiong, "Particle representation for a class of nonlinear SPDEs", *Stochastic Processes and their Applications*, **83**, pp. 103-126, 1999.

[6] M.A. Kouritzin, F. Newton, S. Orsten, D.C. Wilson, "On Detecting Fake Coin Flip Sequences", *IMS Lecture Notes - Monograph Series*, (to appear).